SCIENTIFIC REPRTS

OPEN

Incoherent scattering can favorably influence energy filtering in nanostructured thermoelectrics

Aniket Singha & Bhaskaran Muralidharan

Investigating in detail the physics of energy filtering through a single planar energy barrier in nanostructured thermoelectric generators, we reinforce the non-trivial result that the anticipated enhancement in generated power at a given efficiency via energy filtering is a characteristic of systems dominated by incoherent scattering and is absent in ballistic devices. In such cases, assuming an energy dependent relaxation time $\tau(E) = kE^r$, we show that there exists a minimum value r_{min} beyond which generation can be enhanced by embedding nanobarriers. For bulk generators with embedded nanobarriers, we delve into the details of inter sub-band scattering and show that it has finite contribution to the enhancement in generation. We subsequently discuss the realistic aspects, such as the effect of smooth transmission cut-off and show that for $r > r_{min}$, the optimized energy barrier is just sufficiently wide enough to scatter off low energy electrons, a very wide barrier being detrimental to the performance. Analysis of the obtained results should provide general design guidelines for enhancement in thermoelectric generation via energy filtering. Our non-equilibrium approach is typically valid in the absence of local quasi-equilibrium and hence sets the stage for future advancements in thermoelectric device analysis, for example, Peltier cooling near a barrier interface.

An important direction in the context of electronic engineering to enhance the performance of nanostructured thermoelectric generators[1–10], is to utilize the physics of electronic energy filtering through nanoscale barriers and nanoinclusions[11–24]. To put it simply, energy filtering aims to provide a unidirectional flow of electrons from the hot contact to the cold contact while prohibiting the reverse flow of electrons, which occurs typically when lower energy electrons are scattered off due to the interface potentials[9, 20–22, 25]. In the case of semiconductors, there is the flexibility of varying the equilibrium Fermi energy via appropriate doping. In such a case, a 'good thermoelectric' as schematized in Fig. 1(a) is ideally achieved by tuning the Fermi energy near the conduction band edge so that the resulting transport is devoid of electrons below the Fermi energy. This off-resonant conduction typifies good thermoelectric behavior and has been the object of several initial proposals[1–3, 5, 8]. Such an approach however leads to a drastic reduction in the conductivity while enhancing the Seebeck coefficient. We will refer this as *Approach A*. Energy filtering, as schematized in Fig. 1(b), on the other hand, strives to achieve a desirable performance via engineering nano-barriers[12, 15, 16, 18–23, 26–29]. In this case, the Fermi level resides inside the conduction band and the principal aim is to enhance the Seebeck coefficient by reflecting low energy electrons from the energy barrier. This approach also promotes a unidirectional flow of electrons from the hot contact to the cold contact. We will refer to this as *Approach B*. Ideally, we can say that energy filtering is successful if the latter yields a better performance than the former, especially with a thinner barrier.

While recent works throw some light on this topic[18–24, 26–29], we believe that a few aspects about energy filtering require attention: (1) Most of the current work is based on a linear response analysis of the Seebeck coefficient despite the fact that the regions in the vicinity of the barrier are strongly out of equilibrium. Linear response analysis typically masks the crucial transport physics that determines the delivered terminal power output and efficiency of the generator[30–36]. (2) The role of various scattering mechanisms contributing to the physics of energy filtering is still unclear. (3) A generalized picture of the physics of energy filtering independent of various material parameters is also unclear. In this paper, our focus is hence to develop a general and intuitive understanding of energy filtering and to systematically point out the role played by various scattering mechanisms. Besides that our work uses the non-equilibrium Green's function method which accounts for the non-equilibrium nature of transport and directly evaluates the power and efficiency to provide an overall picture of the device operation.

Department of Electrical Engineering, Indian Institute of Technology Bombay, Powai, Mumbai, 400076, India. Correspondence and requests for materials should be addressed to A.S. (email: aniketsingha@ee.iitb.ac.in)
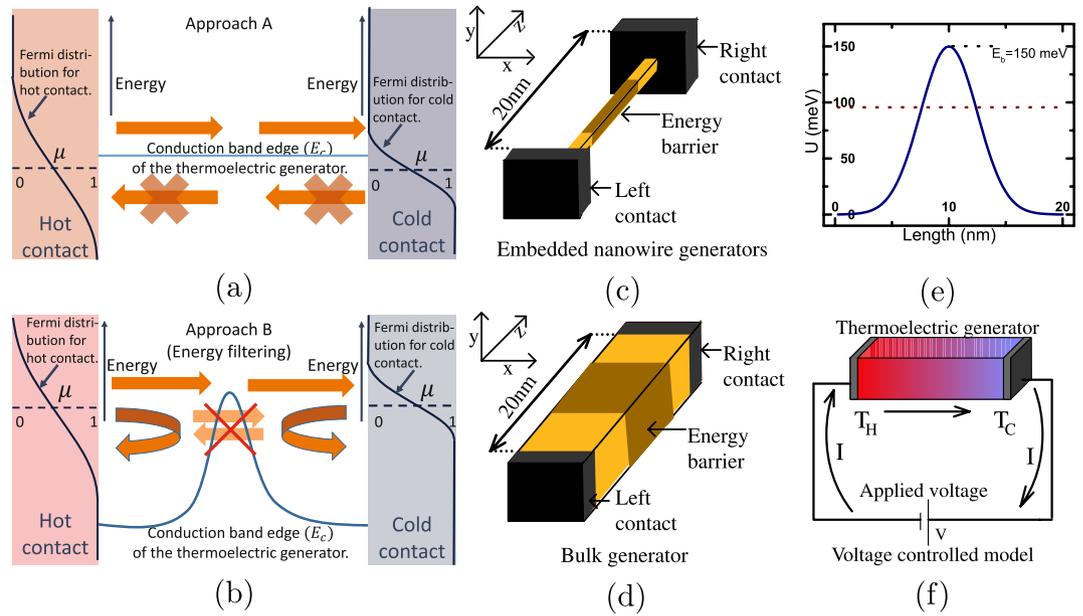
Figure 1. (**a**,**b**) Schematics depicting the two common approaches of improving the thermoelectric performance. (**a**) Approach A: Enhancing the thermoelectric generation by tuning the position of Fermi energy near the conduction band edge and (**b**) Approach B: enhancing the thermoelectric performance by energy filtering via embedding a nano barrier within the thermoelectric generator. The hot and cold contacts are assumed to be macroscopic bodies in equilibrium with the quasi Fermi energy μ at temperature T_H and T_C respectively. (**c**,**d**) The device used for simulation, with a device region of length $20\,nm$ comprising (**c**) embedded nanowire thermoelectric generator (**d**) bulk thermoelectric generator. The shaded region in both the cases represents the embedded barrier (in case of Approach B). (**e**) The band profile of the device region of length $20\,nm$, embedded with a Gaussian energy barrier of height $E_b = 150\,meV$ and width $\sigma_w = 2.7\,nm$. The brown dotted line shows the Fermi energy of the device for the case $E_b - \mu_0 = 2k_BT$. (**f**) Schematic of the voltage controlled model used to simulate the power-efficiency trade-off points.

Our goal here is to present important clarifications on the aforesaid aspects. As a principal contribution, we clarify that the power generation enhancement via energy filtering in both nanowire and bulk devices is dependent on a specific property of the scattering mechanism, which we call *the order of scattering*. It is first shown that for the ballistic case, both Approach A and Approach B lead to an identical performance and hence energy filtering is of limited use. On the other hand, in the diffusive limit for both nanowire and bulk thermoelectric generators, it is shown that the type of scattering mechanism is the principal deciding factor in order to gauge the advantage gained via Approach B. Assuming an energy dependent relaxation time $\tau(E) = kE^r$, we then show that there is a minimum value of the exponent r (termed r_{min}), beyond which energy filtering via Approach B leads to a better enhancement in the generated power compared to Approach A. For such cases, the generated power at a given efficiency increases with an increase in the height of the embedded energy barrier. In addition, we show that for bulk thermoelectric generators with embedded energy barriers, electronic scattering between the high energy and low energy sub-bands enhances the generated power. We also discuss some practical aspects, like the adverse effects of a smooth transmission cut-off due to finite barrier width and investigate further to conclude in case of $r > r_{min}$, the thermoelectric performance peaks when the energy barrier is made *just sufficiently wide enough* to scatter off the low energy electrons.

We utilize the non-equilibrium Green's function (NEGF) formalism to deduce various currents, following which a direct calculation of power and efficiency is performed using the following equations:

$$P = I_C \times V \tag{1}$$

$$\eta = \frac{P}{I_{Qe}}, \tag{2}$$

where I_C is the charge current, I_{Qe} is the electronic heat current at the hot contact and V is the applied voltage assuming a voltage controlled set up described in recent literature[30–36]. Since thermal conductivity due to phonon doesn't vary significantly with the method employed to improve the thermoelectric performance (that is, Approach A or Approach B), we have simplified our calculations in (2) by neglecting the degradation in efficiency due to phonon heat conductivity. We consider thermoelectric generators in which the active regions are smaller than the energy relaxation lengths[18] such that the energy current is almost constant throughout the device region. This assumption simplifies the discussion to a great extent and aids in understanding the physics of energy filtering from an intuitive mathematical viewpoint. For the purpose of the simulations, we use the band parameters of the Δ_2 valley of lightly doped silicon[37] with a longitudinal effective mass, $m_l = m_e$, and a transverse effective mass,

$m_t = 0.2\,m_e$, m_e being the mass of a free electron. The transverse geometries of the device region considered here include bulk, where the transverse extent is infinite and nanowires, where the transverse extent consists of only one sub-band. A schematic of the generic device structure used is shown in Fig. 1(c) for nanowire generators and Fig. 1(d) for bulk generators. The band diagram schematic of our energy filtering based thermoelectric generator is shown in Fig. 1(e). It consists of a 20 nm long doped semiconductor thermoelectric generator with an embedded Gaussian energy barrier (U).

$$U = E_b exp\left(-\frac{(z - z_0)^2}{2\sigma_w^2}\right),$$

where $z_0 = L/2$ is the the mid-point of the device region, L being the total length of the thermoelectric generator. The leads or contacts connected to the 20 nm long device in Fig. 1(c) and (d) are assumed to be reflection-less macroscopic bodies of infinite cross-section, in equilibrium with their respective lattice temperatures and electrochemical potentials (quasi-Fermi levels). For simulation, we use a voltage controlled model, shown in Fig. 1(f), where by varying the bias voltage continuously a the current flow is emulated, to generate a set of points in the the power-efficiency (η) plane[33, 38] for a particular position of the equilibrium electrochemical potential (or equivalently the Fermi energy) μ_0.

In order to assess the relative efficacy of power generation due to energy filtering and compare the relative benefit of Approach B compared to Approach A, we now define a metric called the *filtering coefficient* (λ) defined as

$$\lambda(\eta) = \frac{P_B(\eta)}{P_A(\eta)}, \tag{3}$$

where $P_A(\eta)$ and $P_B(\eta)$ are the maximum power densities obtained at efficiency η via Approach A and Approach B respectively, while $P_A(\eta)$ and $P_B(\eta)$ are taken along the operating line of our device[35]. It should be noted that although we use some specific parameters for simulation, the qualitative discussion as well as the trends noted in the simulated results are general and are valid irrespective of material specific parameters for a particular scattering mechanism.

Results

We now perform a detailed analysis of power generation for Approach A and Approach B using nanowire and bulk thermoelectric generators. The power-efficiency curves are plotted in the η-P plane for several value of the reduced Fermi energy η_f defined as:

$$\eta_f = \begin{cases} \dfrac{E_c - \mu}{k_B T} & \text{for Approach A} \\[2ex] \dfrac{E_c + E_b - \mu}{k_B T} & \text{for Approach } B, \end{cases} \tag{4}$$

E_b being the height of the energy filtering barrier in case of Approach B. In all the discussions to follow, the efficiency of operation will be evaluated relative to the Carnot efficiency given by $\eta_C = 1 - T_C/T_H$.

Energy filtering in the ballistic limit. We start by considering nanowire and bulk thermoelectric generators in the ballistic or coherent limit. We plot, in Fig. 2, the power density versus efficiency curves for a range of η_f for both Approach A and Approach B. In particular, Fig. 2(a–d) depict power generation characteristics for single-moded nanowire generators while Fig. 2(e–h) depict the same for bulk generators. For both nanowire and bulk generators, the maximum power density as well as the power density at a given efficiency for Approach B increase with the width of the energy barrier. The peak performance in this case is achieved for a perfect energy filter with sharp transmission cut-off. This peak performance in Approach B is identical with that of Approach A.

The corresponding filtering coefficients for nanowire and bulk systems, plotted in Fig. 2(d) and (h) respectively, decrease in the high efficiency regime which also corresponds to a high value of η_f. This trend can be attributed to the smooth transmission cut-off at energies close to the barrier height E_b (details in Supplematery material). We hence conclude that in the ballistic limit, for both nanowire or bulk thermoelectric generators, the maximum power generation at a given efficiency is achieved via Approach A. This makes energy filtering via embedded nano barriers of very limited use in the ballistic limit. Hence, in the ballistic limit, when considering generators shorter than the mean free path, energy filtering with a single barrier (Approach B) does not provide any additional benefit over the traditional good thermoelectric generator (Approach A).

Energy filtering in the diffusive limit. *Energy filtering with acoustic phonon scattering.* We turn our attention to the diffusive limit with the inclusion of acoustic phonon scattering and plot in Fig. 3, the filtering analysis of the devices considered previously. In particular, Fig. 3(a–c) demonstrates the generation characteristics for single-moded nanowires and Fig. 3(d–f) demonstrates the power generation characteristics for bulk generators. Contrary to the ballistic limit, acoustic phonon scattering ensures an improved thermoelectric performance in Approach B rather than Approach A. To explain the unusual trends noted in Fig. 3, specifically, the increase in filtering coefficient λ for single-moded nanowire generators with increase in energy barrier height E_b (Fig. 3(c)), we use the parameter Y(E), which is identical to the Boltzmann transport coefficient (details given in supplementary information):

Nanowire generator   Bulk generator
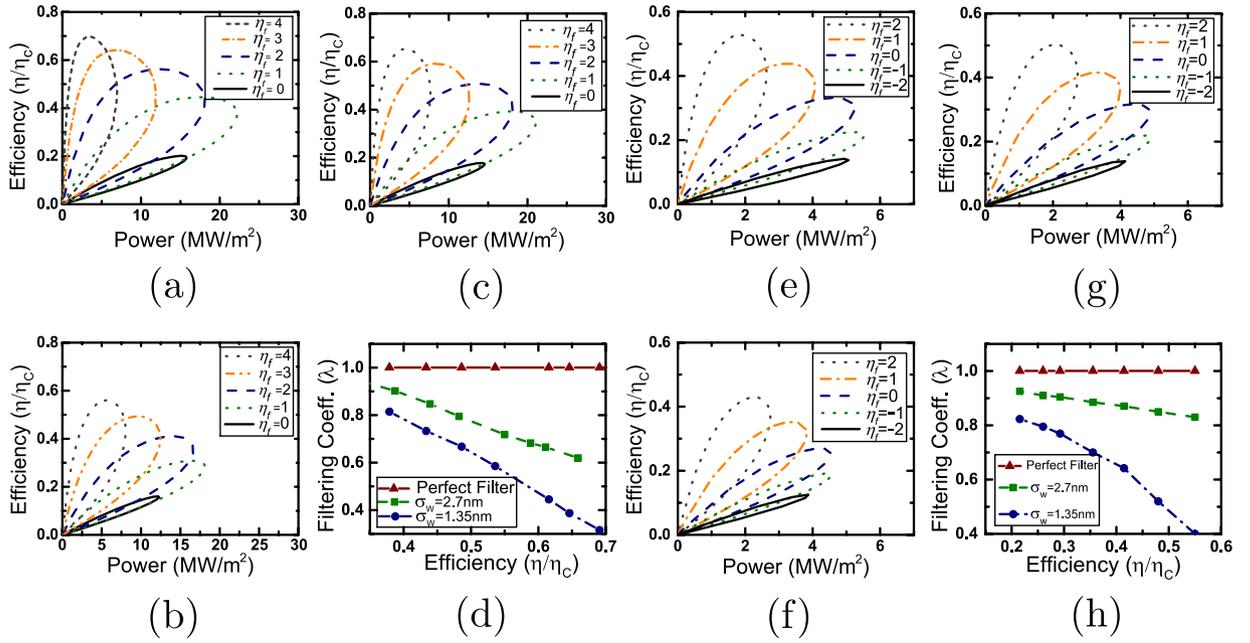
Figure 2. Analysis of energy filtering in the ballistic case. (**a**,**d**) Analysis for a 20 nm long and 2.7 $nm \times$ 2.7 nm ballistic square nanowire: (**a**) Power-efficiency trade-off analysis in case of Approach A for various values of $\eta_f = \frac{E_c - \mu}{k_B T}$. (**b**,**c**) Power-efficiency trade-off analysis in case of Approach B for various values of $\eta_f = \frac{E_c + E_b - \mu}{k_B T}$ (**b**) with a thin energy barrier ($\sigma_w = 1.35\, nm$, $E_b = 150\, meV$), (**c**) with thick barrier ($\sigma_w = 2.7\, nm$, $E_b = 150\, meV$) (**d**) Plot of filtering coefficient (λ) versus efficiency (η/η_C) for a thin, a thick and a perfect energy filtering barrier. (**e**–**h**) Analysis for a 20 nm long bulk generator: (**e**) Power-efficiency trade-off analysis in case of Approach A for various values of $\eta_f = \frac{E_c - \mu}{k_B T}$. (**f**–**g**) Power-efficiency trade-off analysis in case of Approach B for various values of $\eta_f = \frac{E_c - \mu}{k_B T}$ (**f**) with thin barrier ($\sigma_w = 1.35\, nm$, $E_b = 150\, meV$), (**g**) with a thick barrier ($\sigma_w = 2.7\, nm$, $E_b = 150\, meV$) (**h**) Plot of filtering coefficient (λ) versus efficiency (η/η_C) for the bulk generator in case of a thin, a thick and a perfect energy filtering barrier.

$$\Upsilon(E) = v_z^2(E)\tau(E)D_{1D}(E),$$

where $v_z(E)$, $\tau(E)$ and $D_{1D}(E)$ represent the electronic transport velocity, relaxation time and the 1-D density of states respectively. In case of perfect filtering or sharp transmission cut-off, Approach B theoretically ensures an enhanced performance compared to Approach A, with the relative enhancement being an increasing function of the energy barrier height E_b, provided the parameter Y is an increasing function of energy. For bulk thermoelectric generators, under the assumption of uncoupled sub-bands and sharp transmission cut-off, we can define a parameter $\zeta(E) = \frac{\left(E^{\frac{3}{2}} - E_b^{\frac{3}{2}}\right)E^r}{\left\{(E - E_b)^{r + \frac{3}{2}}\right\}}$ with $E > E_b$ to access the relative enhancement in generated power via Approach B compared to Approach A (details given in supplementary information). It can be shown that for acoustic phonon scattering, the parameter $\zeta > 1$, which implies an enhanced generated power via Approach B (details given in supplementary information).

We thus note the non-trivial result that indicates an improvement of thermoelectric performance via energy filtering (Approach B) in the presence of acoustic phonon scattering. Energy filtering is thus beneficial for devices dominated by "acoustic phonon scattering"-like mechanisms $\tau(E) \propto E^{\frac{1}{2}}$ for nanowires and $\tau(E) \propto E^{-\frac{1}{2}}$ for bulk) when they are longer than the mean free path. We now explore what happens for the higher order scattering mechanisms.

Energy filtering with higher order scattering mechanisms. A scattering mechanism, with relaxation time given by $\tau(E) = k_0 E^r$, is said to be of order '$-r$', with a lower value of the exponent r denoting a higher order scattering process. For acoustic phonon scattering, the relaxation time is given by $\tau(E) \approx k_o E^{\frac{1}{2}}$ in the case of nanowires and $\tau(E) \approx k_o E^{-\frac{1}{2}}$ in the bulk case. Then, the question arises, what is the effect of r on the filtering coefficient? Another related question is, if there is a minimum value of r, termed r_{min}, beyond which energy filtering viz. Approach B ensures an enhanced performance compared to approach A?

Nanowire generator

Bulk generator
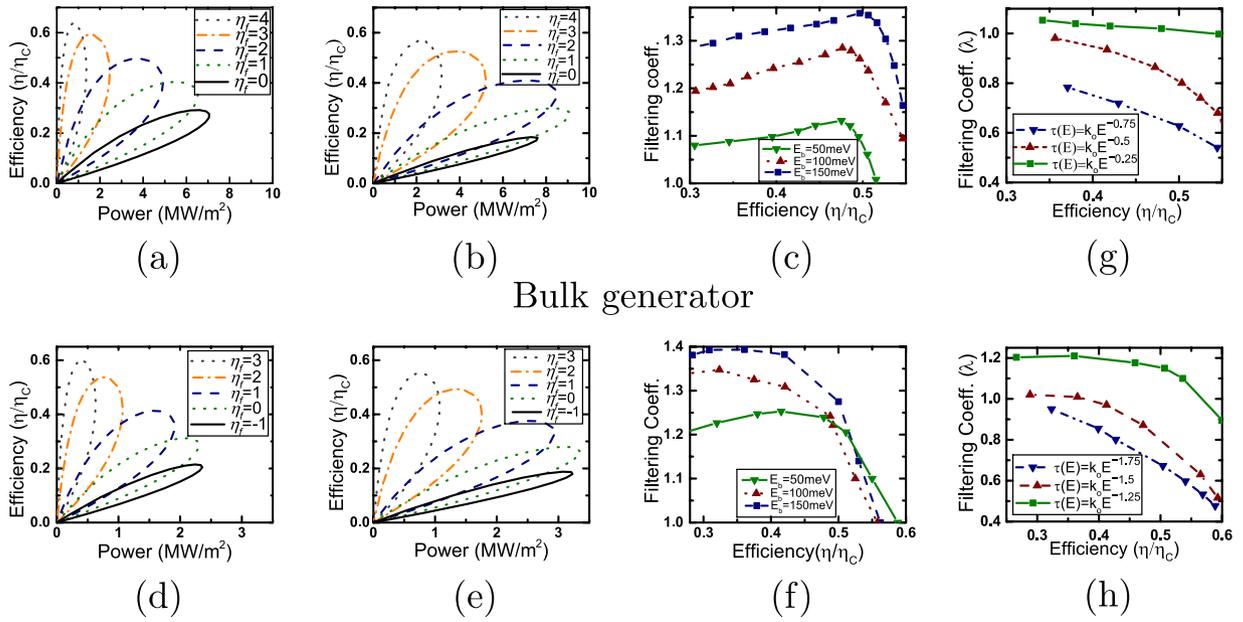
Figure 3. Thermoelectric generation and filtering coefficient analysis with incoherent scattering mechanisms (**a**–**c**) Analysis for a square nanowire of length 20 *nm* and width 2.7 *nm* with the inclusion of acoustic phonon scattering: (**a**) Power-efficiency trade-off analysis in case of Approach A for various values of $\eta_f = \frac{E_c - \mu}{k_B T}$. (**b**) Power-efficiency trade-off analysis in case of Approach B for various values of $\eta_f = \frac{E - E_c - E_b}{k_B T}$ ($E_b = 150\, meV$ and $\sigma_w = 2.7\, nm$). (**c**) Filtering coefficient plotted for various heights of the energy filtering barrier. (**d**–**f**) Analysis for a bulk generator of length 20 *nm* with the inclusion of acoustic phonon scattering: (**d**) Power-efficiency trade-off analysis in case of Approach A for various values of $\eta_f = \frac{E_c - \mu}{k_B T}$. (**e**) Power-efficiency trade-off analysis in case of Approach B for various values of $\eta_f = \frac{E - E_c - E_b}{k_B T}$ ($E_b = 150\, meV$ and $\sigma_w = 2.7\, nm$). (**f**) Filtering coefficient plotted for various heights of the energy filtering barrier. (**g**–**h**) Filtering coefficients plotted for higher order scattering mechanisms with Gaussian energy barriers ($\sigma_w = 2.7\, nm$, $E_b = 150\, meV$) for (**g**) nanowire generator with dimensions used in (**a**–**c** and **h**) bulk generator with dimensions used in (**d**–**f**).

As already discussed, for single-moded nanowires, Approach B always ensures an enhanced thermoelectric performance when the parameter $Y(E)$ is an increasing function of energy (details given in supplementary information), provided that energy filtering is perfect. Hence, in the case of non-parabolic bands or in the case where different scattering mechanisms dominate, the height of the energy barrier, for optimum performance, should be approximately identical to the energy at which the rate of increase of $D\tau v_z^2$ saturates. The optimum doping for such a case should fix the Fermi level close to the energy barrier height depending on the desired efficiency. The rate of increase of $Y(E)$ with energy determines the relative advantage gained via Approach B, that is, for the same energy barrier height with $\tau(E) = kE^r$ and parabolic dispersion, filtering coefficient at a given efficiency is an increasing function of r. For a single-moded nanowire, $v_z^2(E) = \frac{2E}{m_l}$ and $D(E) = \frac{1}{\hbar \pi}\sqrt{\frac{m_l}{2E}}$, implying $r_{min} = -\frac{1}{2}$. For $r < r_{min}$, Approach A leads to an optimized power generation degrading the filtering coefficient less than unity. An analytical calculation of r_{min} for bulk generators is not trivial due to inter sub-band coupling. However, assuming uncoupled sub-bands and perfect energy filtering, for $E_b = 150\, meV$, it can be shown that Approach B is advantageous for $r \gtrsim -0.7$. (see supplementary information). We hence note that in case of devices longer than the mean free path, the benefit obtained from energy filtering decreases as the order of the dominating scattering mechanism increases.

We plot, in Fig. 3(g) and (h), the filtering coefficient (λ) versus efficiency (η/η_C) for nanowire and bulk generators affected by scattering mechanisms of order higher than that of acoustic phonon scattering. The filtering coefficient vs. efficiency plots in Fig. 3(h) indicate that for bulk thermoelectric generators, the calculated upper bound $r_{min} = -0.7$ under the simplified assumption of uncoupled sub-bands is indeed an overestimate. To explain this behavior, we thus need to delve into the details of inter sub-band scattering and understand its contribution to power generation.

Role of intermode coupling in bulk generators. We now uncover the role of coupling between the various transverse sub-bands in the bulk case, in particular, the role of incoherent scattering in enhancing the filtering coefficient. Conservation of lateral momentum in the ballistic limit implies that, electrons from the high energy transverse sub-bands are reflected from the energy barrier[39–43] and hence cannot contribute to the generated power. However, in the diffusive limit, transverse sub-bands are coupled which may result in an electronic
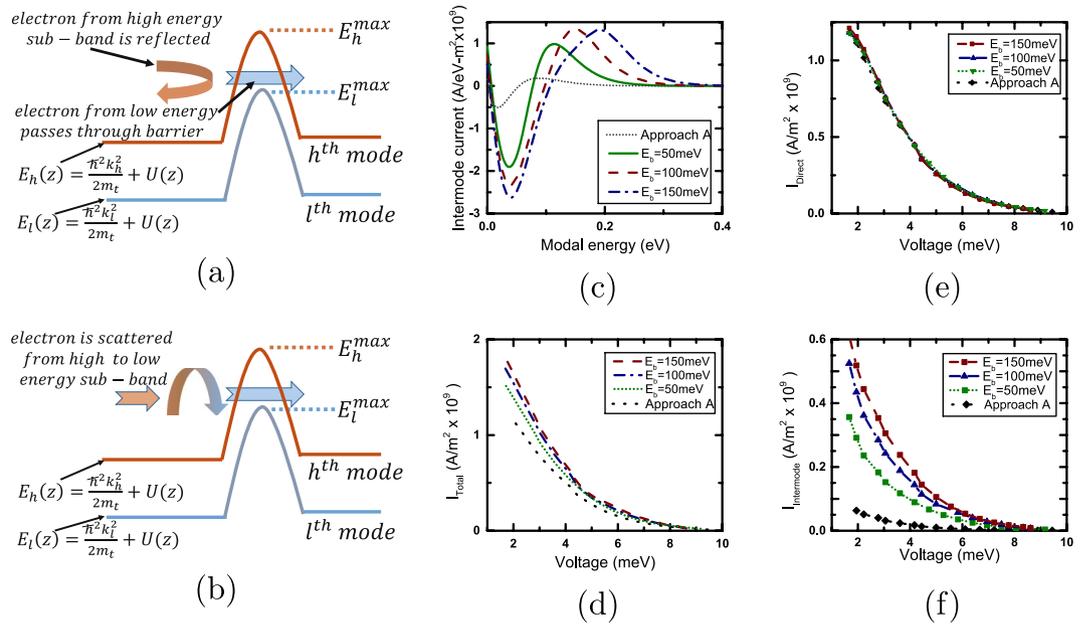
Figure 4. Demonstration of performance improvement due to inter sub-band coupling in energy filtering based bulk thermoelectric generators. (**a,b**) Schematic diagram illustrating electronic transport through a device with two sub-bands: the lth and the hth sub-band with lateral momentum $\hbar k_l$ and $\hbar k_h$ respectively. (**a**) Electronic transport when the sub-bands are uncoupled. In this case, the electrons from the hth sub-band are completely reflected from the barrier if the total energy of the electron is lower than E_h^{max}. (**b**) Electronic transport when the sub-bands are coupled. In this case, the electrons from the hth sub-band (with energy between E_l^{max} and E_h^{max}) may be scattered to the low energy sub-bands between the hot contact and the barrier interface and subsequently flow towards the cold contact. (**c**) Plot of intermode coupling current vs. modal (sub-band) energy per unit area per unit energy in case of bulk generators at the maximum power. (**d–f**) Current profiles per unit area at the maximum power at different bias voltages (V) considering acoustic phonon scattering. Plot of (**d**) the total current, (**e**) the current propagating directly between the contacts without changing sub-bands and (**f**) the intermode coupling current. Simulations are done for a 20 nm long device. For Approach B, an embedded Gaussian energy barrier is used ($\sigma_w = 2.7$ nm). An enhancement in generated power with barrier height results from an enhancement in the intermode coupling current.

flow between them. The net scattering current between the sub-bands is however dictated by the relative non-equilibrium conditions of the respective sub-bands and will henceforth be referred to as the *intermode coupling current*. Such a flow of the intermode coupling current between the sub-bands occurs in the region between the hot contact and the barrier interface. This current subsequently flows to the cold contact and can significantly enhance the generated power in the case of energy filtering.

The situation described above is schematically illustrated in Fig. 4(a) and (b) considering electronic transport through two sub-bands with transverse momentum $\hbar k_l$ and $\hbar k_h$. In the classical limit the approximate transmission cut-off of these modes are E_l^{max} and E_h^{max} respectively. Incoherent scattering can drive an electron (which would otherwise be reflected from the energy barrier) with energy $E_l^{max} < E < E_h^{max}$ from the hth sub-band to the lth sub-band and contribute to the current flow. For bulk thermoelectric generators the density of sub-bands $M(E) = \frac{m_t}{2\pi\hbar^2}(E - E_C)$ increases with energy resulting in an increase in the intermode coupling current with the energy barrier height.

We plot in Fig. 4(c), the energy resolved intermode coupling current per unit area at the maximum power for various barrier heights taking acoustic phonon scattering into account. The electronic current flows out (positive value) of the higher energy sub-bands into (negative value) the lower energy modes. We plot in Fig. 4(d–f), the different current profiles at the maximum power at different voltage biases. The total current per unit area (I_{Total}) at the cold contact consists of two parts: (a) the direct current (I_{Direct}) that flows per unit area from the hot contact to the cold contact without changing sub-bands (b) the intermode coupling current $I_{Intermode}$ that flows per unit area from the higher energy sub-bands to the lower energy sub-bands between the hot contact and the energy barrier interface and consequently flows toward the cold contact. Figure 4(e) demonstrates that I_{Direct} remains almost unchanged with an increase in the height of the energy barrier. Hence, the increase in the generated power with the height of the energy barrier in this case is attributed to an increase in $I_{Intermode}$ as shown in Fig. 4(f). Such an enhancement in generated power due to intermode coupling current is dependent on incoherent scattering and is absent in the ballistic limit.

Optimizing the filtering coefficient in the diffusive limit.
In this section, we reinforce that in the diffusive limit for $r > r_{min}$, the filtering coefficient tends to maximize when the barrier width is 'just sufficient' to
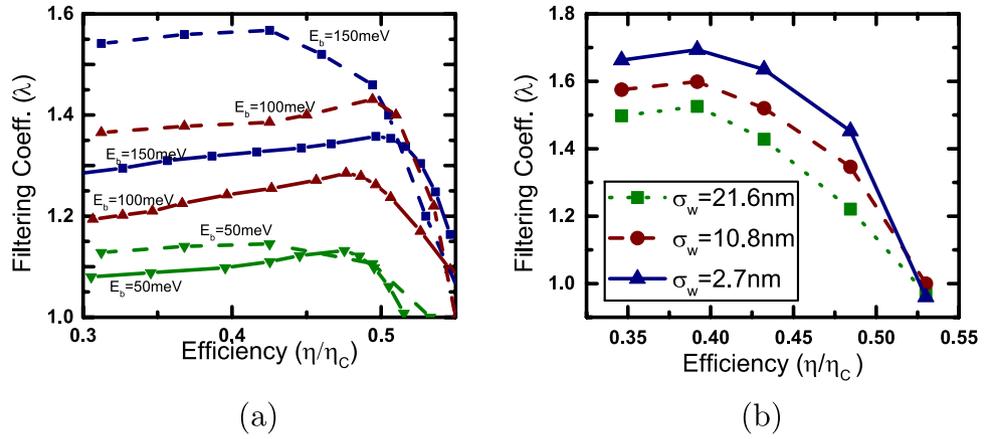
Figure 5. Demonstration of the optimum conditions under which energy filtering should be employed. (**a**) Demonstration of the enhancement in the filtering coefficient when the total length of the generator is much greater than the width of the energy filtering barrier. Plot of the filtering coefficient (λ) versus efficiency (η/η_C) for various barrier heights in case of 2.7 *nm* wide square nanowires of length 20 *nm* (solid curves) and 40 *nm* (dashed curves). The nanowires are embedded with a Gaussian energy barrier ($\sigma_w = 2.7$ *nm*). (**b**) Demonstration of deterioration of filtering coefficient when the width of the energy barrier is increased compared to the minimum width necessary to block an appreciable reverse flow of electrons from the cold contact. Filtering coefficient versus efficiency (η/η_C) for a 170 *nm* long diffusive nanowire with different energy barrier widths (with $E_b = 150$ *meV*) taking acoustic phonon scattering into account.

block an appreciable reverse flow of electrons from the cold contact to the hot contact, a wider barrier than the optimized one being detrimental to the thermoelectric performance.

Dependence of the filtering coefficient on device length.   For both nanowire and bulk generators with $r > r_{min}$, Y(E) is minimum at the top of the energy barrier when energy filtering viz. Approach B is employed. Hence, Approach B is most useful when the device region between either of the contacts and the barrier interface is much longer compared to the width of the energy barrier. Such a design facilitates most of the electronic transport in the region where the kinetic energy and Y(E) are very high. This effect is demonstrated in Fig. 5(a) where it is shown that for the same energy barrier width, the filtering coefficient increases for longer generators.

Optimized energy barrier for maximizing the filtering coefficient.   While it is obvious that a very thin energy barrier adversely affects the thermoelectric performance due to reverse flow of electrons, a very wide barrier is also detrimental to the thermoelectric performance due to decrease in the parameter Y(E) at the top of the barrier resulting in an overall decrease in the transmission probability (details in supplementary material). This phenomenon is demonstrated in Fig. 5(b) taking incoherent (acoustic phonon) scattering into account where it is shown that barriers wider than 2.7 *nm* are detrimental to the thermoelectric performance.

Hence, we conclude that for Approach B with $r > r_{min}$, the optimum energy filtering barrier is 'just sufficiently wide' to block an appreciable reverse flow of electrons from the cold contact to the hot contact, the suitable generator length for employing energy filtering being at least a few times greater than the optimum barrier width.

Impact of phonon heat conduction.   So far, in the above discussion, we have neglected the effect of phonon heat conduction. In realistic thermoelectric generators, however, the efficiency of operation is often limited by phonon or lattice heat conduction[44–49] if

$$I_{Qp} \gg I_{Qe},\tag{5}$$

where I_{Qp} and I_{Qe} are the heat currents due to phonon and electronic conduction respectively at the hot contact. The efficiency of operation in this case is given as:

$$\eta = \frac{P}{I_{Qp} + I_{Qe}} \approx \frac{P}{I_{Qp}}.\tag{6}$$

The expressions (5) and (6) naturally question the validity of our investigation where I_{Qp} is neglected.

Hence, we extend our proposed theory to the case where heat conduction is dominated by lattice heat conductance. In the case where $I_{Qpp} \gg I_{Qe}$, the operating point with maximum power becomes identical to the operating point with maximum efficiency. In this case, we define two parameters which may be used to gauge the relative advantage gained via Approach B compared to Approach A.

$$\rho = \frac{P_B^{MAX}}{P_A^{MAX}}$$
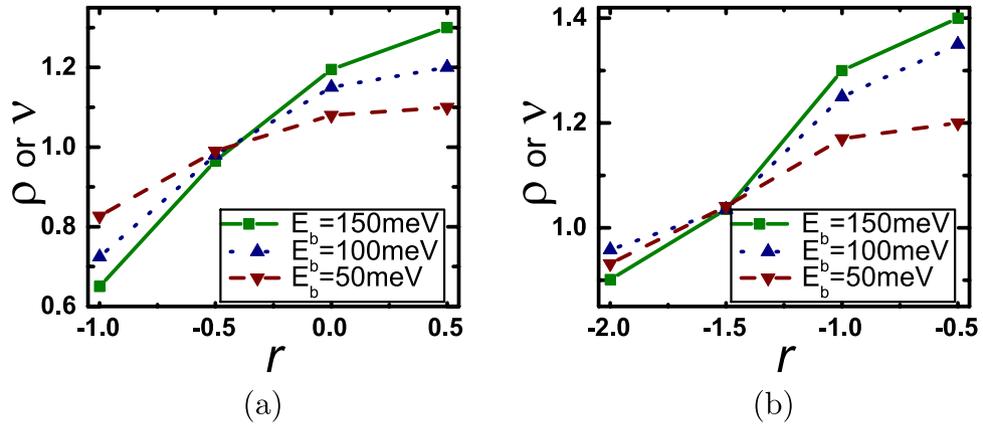
Figure 6. Analysis of performance improvement in thermoelectric generators via energy filtering under the condition $I_{Qp} \gg I_{Qe}$ (heat conduction dominated by phonon). Plot of ρ vs. r for (**a**) a single moded square nanowire of length 20 *nm* and width 2.7 *nm* and (**b**) a bulk generator of length 20 *nm*. The generators are embedded with a Gaussian energy barrier ($\sigma_w = 2.7$ *nm*). Plots are shown for three different energy barrier heights (E_b).

$$\nu = \frac{\eta_{P_{MAX}}^{B}}{\eta_{P_{MAX}}^{A}} \approx \frac{P_B^{MAX}}{P_A^{MAX}},$$

where $P_{A(B)}^{MAX}$ and $\eta_{P_{MAX}}^{A\ (B)}$ are the maximum power generated via Approach A(B) and the efficiency at the maximum generated power in case of Approach A(B) respectively.

We plot, in Fig. 6(a) and (b), ρ vs. r for nanowire and bulk thermoelectric generators respectively in the limiting case of $I_{Qp} \gg I_{Qe}$ for various heights of the energy filtering barrier. ρ or ν increase monotonically with an increasing value of r. In case of perfect filtering in nanowires, Approach B ensures an enhanced performance compared to Approach A in terms of maximum power generation when Y(E) is an increasing function of energy. For such cases, both ρ and ν increase with the height of the energy barrier. This general trends in ρ or ν for nanowires are also manifested in bulk generators for the case $I_{Qp} \gg I_{Qe}$. We hence note that preceding discussion on energy filtering is valid even in the limit where lattice heat conduction dominates.

Discussion

So far, we have discussed the general conditions under which energy filtering enhances generated power in nanoscale and bulk thermoelectric generators. To demonstrate such conditions we have assumed smooth Gaussian barriers. However our discussion is valid for energy filtering achieved via other means, for example, embedding nanoinclusions randomly throughout the generator. Although disproven theoretically[21], such nanoinclusions are generally thought to create resonant states which can further aid in enhancing the efficiency of thermoelectric generation. In realistic devices, a number of electronic scattering mechanisms may be dominant such that the relaxation time of the electrons is a polynomial function of kinetic energy (E).

$$\tau(E) \approx \sum_i k_i E^{r_i}$$

We split the contributions r_i into two groups (a) $r_i \geq r_{min}$ (b) $r_i < r_{min}$. With energy filtering, thermoelectric power generation is enhanced in the presence of the scattering mechanisms satisfying $r_i \geq r_{min}$ while the same is degraded in the presence of the scattering mechanisms satisfying $r_i < r_{min}$. In a case where both types of scattering mechanisms are dominant or the energy band is non-parabolic, there is an optimum height of the energy filtering barrier at which the enhancement of generated power is maximum in the case of Approach B[20]. The optimum barrier height in such a case should approximately be identical to the energy at which the parameter $D\tau v_z^2$ starts to saturate, the optimum position of the Fermi energy being in the range of a few $k_B T$ with respect to the top of the energy barrier depending on the desired efficiency. Our discussion in this paper, although general, should provide a qualitative idea on the physics of the enhancement in generated power via energy filtering in the ballistic and the diffusive limit and hence should provide general optimization guidelines for thermoelectric generators with material specific properties.

Methods

In order to perform the transport calculations to be presented, we employ the NEGF transport formalism under the self-consistent Born approximation[40, 50] to incorporate scattering in the device region (details given in the supplementary material). We employ the single particle Green's function $G(\vec{k}_m, E)$, for each transverse sub-band m[40], evaluated from the device Hamiltonian matrix [H] given by:

Parameters	Values	Parameters	Values
$T_H\ (k_B T_H)$	330 K (28.435 meV)	Length of device	20 nm
$T_C\ (k_B T_C)$	300 K (25.85 meV)	D_O (SI)	$0.2\ F\,eV^2$
$T = \frac{T_H + T_C}{2} (k_B T)$	315K (27.1425 meV)	$S(E)$ (SI)	$\frac{2\pi D_O}{\hbar}\left(10\frac{E}{e}\right)^{-u} eV^2$
m_l	m_e	a (lattice constant)	2.7 Å
m_t	$0.2\,m_e$	E_c	$0\,eV$

Table 1. Parameters used for simulation in this paper. *Note:* "SI" = supplementary information. $F = \frac{1}{N_x N_y}$, N_x and N_y being the number of lattice points in the *x* and *y* directions with electronic transport being in the *z*− direction. The parameter *u* is related to the order of scattering process '−r' by the equation $u = -r + \frac{1}{2}$ for nanowires and $u = -r - \frac{1}{2}$ for bulk generators. $u = 0$ for acoustic phonon scattering. m_e is the free electron mass and D_O is related to the acoustic deformation potential (see supplementary information).

$$G(\vec{k}_m, E) = [EI - H - U - E_m - \Sigma(\vec{k}_m, E)]^{-1},$$
$$\Sigma(\vec{k}_m, E) = \Sigma_L(\vec{k}_m, E) + \Sigma_R(\vec{k}_m, E) + \Sigma_s(\vec{k}_m, E), \tag{7}$$

where $[H] = [H_0] + U$, with $[H_0]$ being the device tight-binding Hamiltonian matrix constructed using effective mass approach[40] and *I* being the identity matrix of the same dimension as the Hamiltonian. The free variable denoting the energy of electronic wavefunction is *E* and the spatial variation in the conduction band minimum is described by the matrix *U*. The sub-band energy of the mth sub-band is $E_m = \frac{\hbar^2 k_m^2}{2m_t}$. The vector $\vec{k}_m$ represents the wavevector of the electron in the transverse direction for the mth mode. The net scattering self energy matrix $[\Sigma(\vec{k}_m, E)]$ includes that due to the scattering of the electronic wavefunctions from the contacts into the device region, denoted by $\Sigma_L(\vec{k}_m, E) + \Sigma_R(\vec{k}_m, E)$ as well as the scattering of electronic wavefunctions inside the device due to incoherent processes such as phonons and non-idealities, denoted by $\Sigma_s(\vec{k}_m, E)$ (detailed in the supplementary information). The calculation of the in-scattering and the out-scattering functions involve a self consistent procedure, (detailed in the supplementary information), with the electron and the hole density operators $G^n(\vec{k}_m, E), G^p(\vec{k}_m, E)$ defined as

$$G^n(\vec{k}_m, E) = G(\vec{k}_m, E)\Sigma^{in}(\vec{k}_m, E)G^\dagger(\vec{k}_m, E),$$
$$G^p(\vec{k}_m, E) = G(\vec{k}_m, E)\Sigma^{out}(\vec{k}_m, E)G^\dagger(\vec{k}_m, E). \tag{8}$$

Upon convergence of the self-consistent quantities, the charge and heat currents are evaluated in the lattice basis as:

$$I_C^{j\rightarrow j+1} = \sum_{k_m} i\frac{e}{\pi\hbar} \int [G_{j+1,j}^n(\vec{k}_m, E)H_{j,j+1}(E) - H_{j+1,j}(E)G_{j,j+1}^n(\vec{k}_m, E)]dE, \tag{9}$$

$$I_Q^{j\rightarrow j+1} = \sum_{k_m} \frac{i}{\pi\hbar} \times \int (E - \mu_H)[G_{j+1,j}^n(\vec{k}_m, E)H_{j,j+1}(E) - H_{j+1,j}(E)G_{j,j+1}^n(\vec{k}_m, E)]dE, \tag{10}$$

where μ_H is the electrochemical potential of the hot contact, M_{ij} is a generic matrix element of the concerned operator between two lattice points *i* and *j*. In the tight-binding scheme used here, we only consider the next nearest neighbor such that $j = i \pm 1$. A list of parameters used for the simulation of the NEGF equations are given in Table 1.

References
1. Hicks, L. D. & Dresselhaus, M. S. Effect of quantum-well structures on the thermoelectric figure of merit. *Phys. Rev. B* **47**(19), 12727 (1993).
2. Hicks, L. D. & Dresselhaus, M. S. Thermoelectric figure of merit of a one-dimensional conductor. *Phys. Rev. B* **47**, 16631 (1993).
3. Dresselhaus, M. S. *et al. Adv. Mat*er. **19**, 1043, 2007.
4. Goldsmid. *Introduction to Thermoelectricity*. Springer, 2009.
5. Mahan, G. D. & Sofo, J. O. The best thermoelectric. *Proceedings of National Academy of Sciences of the United States of America* **93**(15), 7436–7439 (1996).
6. Poudel, B. *et al*. High-Thermoelectric Performance of Nanostructured Bismuth Antimony Telluride Bulk Alloys. *Science* **320**, 634 (2008).
7. Snyder, G. J. & Toberer, E. S. Complex thermoelectric materials. *Nat. Mater.* **7**, 105 (2008).
8. Heremans, J. P. *et al*. Enhancement of Thermoelectric Efficiency in PbTe by Distortion of the Electronic Density of States. *Science* **321**, 554 (2008).
9. Zebarjadi, M. *et al*. Power factor enhancement by modulation doping in bulk nanocomposites. *Nano Letters* **11**(6), 2225–2230 (2011).
10. Natalya, A. Zimbovskaya. Seebeck effect in molecular junctions. *Journal of Physics: Condensed Matter* **28**(18), 183002 (2016).
11. Thesberg, M., Kosina, H. & Neophytou, N. On the effectiveness of the thermoelectric energy filtering mechanism in low-dimensional superlattices and nano-composites. *Journal of Applied Physics* **120**(23), 234302 (2016).

12. Mi, J. L., Zhao, X. B., Zhu, T. J. & Tu, J. P. Thermoelectric properties of $Yb_{0.15}Co_4Sb_{12}$ based nanocomposites with $CoSb_3$ nano-inclusion. *Journal of Physics D: Applied Physics* **41**(20), 205403 (2008).
13. Li, J. F., Liu, W. S., Zhao, L. D. & Zhou, M. High-performance nanostructured thermoelectric materials. *NPG Asia Mater* **2**, 152–158 (2010).
14. Sumithra, S. *et al.* Effect of nite nanoinclusions on thermoelectric properties of Bi_2Te_3. *Journal of Electronic Materials* **41**(6), 1401–1407 (2012).
15. Lin, H., Božin, E. S., Billinge, S. J. L., Quarez, E. & Kanatzidis, M. G. Nanoscale clusters in the high performance thermoelectric $AgPb_mSbTe_{m+2}$. *Phys. Rev. B* **72**, 174113 (2005).
16. Zide, J. M. *et al.* Thermoelectric power factor in semiconductors with buried epitaxial semimetallic nanoparticles. *Applied Physics Letters*, **87**(11) 2005.
17. Heremans, J. P., Thrush, C. M. & Morelli, D. T. Thermopower enhancement in pbte with pb precipitates. *Journal of Applied Physics*, **98**(6) 2005.
18. Kim, R & Lundstrom, M. S. Computational study of energy filtering effects in one-dimensional composite nano-structures. *Journal of Applied Physics*, **111**(2) 2012.
19. Kim, R & Lundstrom, M. S. Computational study of the seebeck coefficient of one-dimensional composite nano-structures. *Journal of Applied Physics*, **110**(3) 2011.
20. Bahk, J. H., Bian, Z. & Shakouri, A. Electron energy filtering by a nonplanar potential to enhance the thermoelectric power factor in bulk materials. *Phys. Rev. B* **87**, 075204 (2013).
21. Faleev, S. V. & Léonard, F. Theory of enhancement of thermoelectric properties of materials with nanoinclusions. *Phys. Rev. B* **77**, 214304 (2008).
22. Neophytou, N. & Kosina, H. Optimizing thermoelectric power factor by means of a potential barrier. *Journal of Applied Physics*, **114**(4) 2013.
23. Martin, J., Wang, L., Chen, Lidong & Nolas, G. S. Enhanced seebeck coefficient through energy-barrier scattering in pbte nanocomposites. *Phys. Rev. B* **79**, 115311 (2009).
24. Berland, K. *et al.* Enhancement of thermoelectric properties by energy filtering: Theoretical potential and experimental reality in nanostructured znsb. *Journal of Applied Physics*, **119**(12) 2016.
25. Vashaee, D. & Shakouri, A. Improved thermoelectric power factor in metal-based superlattices. *Phys. Rev. Lett.* **92**, 106103 (2004).
26. Popescu, A., Woods, L. M., Martin, J. & Nolas, G. S. Model of transport properties of thermoelectric nanocomposite materials. *Phys. Rev. B* **79**, 205302 (2009).
27. Neophytou, N. *et al.* Power factor enhancement by inhomogeneous distribution of dopants in two-phase nanocrystalline systems. *Journal of Electronic Materials* **43**(6), 1896–1904 (2014).
28. Thesberg, M., Pourfath, M., Kosina, H. & Neophytou, N. The influence of non-idealities on the thermoelectric power factor of nanostructured superlattices. *Journal of Applied Physics* **118**(22), 224301 (2015).
29. Yoshimasa, N. and Tohru Hirano. Improvement of the efficiency of thermoelectric energy conversion by utilizing potential barriers. *Japanese Journal of Applied Physics* **36**(1R), 170 (1997).
30. Leijnse, M., Wegewijs, M. R. & Flensberg, K. Nonlinear thermoelectric properties of molecular junctions with vibrational coupling. *Phys. Rev. B* **82**, 045412 (2010).
31. Sothmann, B., Sánchez, R. & Jordan, A. N. Thermoelectric energy harvesting with quantum dots. *Nanotechnology* **26**, 32001 (2014).
32. Muralidharan, B. & Grifoni, M. Performance analysis of an interacting quantum dot thermoelectric setup. *Phys. Rev. B* **85**, 155423 (2012).
33. Nakpathomkun, N., Xu, H. Q. & Linke, H. Thermoelectric efficiency at maximum power in low-dimensional systems. *Phys. Rev. B* **82**, 235428 (2010).
34. Choi, Y. & Jordan, A. N. Three-terminal heat engine and refrigerator based on superlattices. *Physica E* **74**, 465 (2016).
35. Singha, A., Mahanti, S. D. & Muralidharan, B. Exploring packaging strategies of nano-embedded thermoelectric generators. *AIP Advances*, **5**(10) 2015.
36. Agarwal, A. & Muralidharan, B. Power and efficiency analysis of a realistic resonant tunneling diode thermoelectric. *Applied Physics Letters* **105**(1), 013104 (2014).
37. Esseni, L.S.D., Palestri, P. Nanoscale MOS Transistors Semi-Classical Transport and Applications. Cambridge, 2011.
38. Whitney, R. S. Most Efficient Quantum Thermoelectric at Finite Power Output. *Physical Review Letters* **112**(13), 130601 (2014).
39. Datta, S. *Electronic Transport in Mesoscopic Systems*. Cambridge University Press, 1997.
40. Datta, S. *Quantum Transport:Atom to Transistor*. Cambridge Press, 2005.
41. Datta, S. Lessons from nanoelectronics: a new perspective on transport. *Lessons from nanosciences: A lecture note series*. (World Scientific, Singapore, 2012).
42. Vashaee, D. & Shakouri, A. Conservation of lateral momentum in heterostructure integrated thermionic coolers. *MRS Proceedings* **691**, 001 (2001).
43. Kim, R., Jeong, C. & Lundstrom, M. S. On momentum conservation and thermionic emission cooling. *Journal of Applied Physics*, **107**(5) 2010.
44. Mingo, N. & Broido, D. A. Lattice thermal conductivity crossovers in semiconductor nanowires. *Phys. Rev. Lett.* **93**, 246106 (2004).
45. Mingo, N. Thermoelectric figure of merit and maximum power factor in iii–v semiconductor nanowires. *Applied Physics Letters* **84**(14), 2652–2654 (2004).
46. Zhou, F. *et al.* Determination of transport properties in chromium disilicide nanowires via combined thermoelectric and structural characterizations. *Nano Letters* **7**(6), 1649–1654 (2007).
47. Zhou, F. *et al.* Effect of growth base pressure on the thermoelectric properties of indium antimonide nanowires. *Journal of Physics D: Applied Physics* **43**(2), 025406 (2010).
48. Boukai, A. I. *et al.* Silicon nanowires as efficient thermoelectric materials. *Nature* **451**, 168–171 (2008).
49. Hochbaum, A. I. *et al.* Enhanced thermoelectric performance of rough silicon nanowires. *Nature Publishing Group* **451**, 163–167 (2008).
50. Lake, R. & Datta, S. Energy balance and heat exchange in mesoscopic systems. *Phys. Rev. B* **46**, 4757–4763 (1992).

Acknowledgements

Author Contributions

A.S. conceived the idea. A.S. and B.M. contributed to the mathematical analysis, simulations, development of the blue prints and the writing of the paper. A.S. and B.M. extensively discussed the science, the simulations and the results obtained.

Additional Information

Supplementary information accompanies this paper at doi:10.1038/s41598-017-07935-w

Competing Interests: The authors declare that they have no competing interests.

Publisher's note: Springer Nature remains neutral with regard to jurisdictional claims in published maps and institutional affiliations.